photonics

MDPI

Article

Hybrid Adaptive Bias OFDM-Based IM/DD Visible Light Communication System

Huandong Hong † and Zhengquan Li *,†

Jiangsu Provincial Engineering Laboratory of Pattern Recognition and Computational Intelligence, Jiangnan University, Wuxi 214122, China; 6191918015@stu.jiangnan.edu.cn

* Correspondence: lzq722@jiangnan.edu.cn; Tel.: +86-138-6183-7081

† These authors contributed equally to this work.

Abstract: Conventional optical orthogonal frequency division multiplexing (OFDM) schemes, such as adaptively biased optical OFDM (ABO-OFDM) and hybrid asymmetrically clipped optical OFDM (HACO-OFDM), are unable to tap all the resources of the subcarriers and only achieve relatively high power efficiency. In this paper, a hybrid adaptive bias optical OFDM (HABO-OFDM) scheme for visible light communication (VLC) is proposed to improve spectral efficiency and power efficiency. In the proposed HABO-OFDM scheme, different optical OFDM components are combined for transmission at the same time, and the adaptive bias is designed to ensure the non-negativity, as well as obtaining significantly high power efficiency. Meanwhile, the implementation complexity of the HABO-OFDM receiver is notably lower than the conventional superimposed optical OFDM schemes. Simulation results show that the proposed HABO-OFDM scheme outperforms ABO-OFDM and HACO-OFDM in terms of both peak-to-average-power ratio (PAPR) and power efficiency. The PAPR performance of HABO-OFDM is about 3.2 dB lower than that of HACO-OFDM and 1.7 dB lower than that of ABO-OFDM. Moreover, we can see that the $E_{b(elec)}/N_0$ required for HABO-OFDM to reach the BER target is lower than the other two schemes at the Bit rate/Normalized bandwidth range of 3.5 to 8.75, which means that the power efficiency of HABO-OFDM is higher in this range.

Keywords: orthogonal frequency division multiplexing (OFDM); visible light communication (VLC); power efficiency; peak-to-average-power ratio (PAPR)

Citation: Hong, H.; Li, Z. Hybrid Adaptive Bias OFDM-Based IM/DD Visible Light Communication System. *Photonics* **2021**, *8*, 257. https://doi.org/10.3390/photonics8070257

Received: 9 June 2021
Accepted: 30 June 2021
Published: 5 July 2021

1. Introduction

With the rapid increase in wireless mobile devices, the continuous increase of wireless data traffic has brought challenges to the continuous reduction of radio frequency (RF) spectrum, which has also driven the demand for alternative technologies [1,2]. In order to solve the contradiction between the explosive growth of data and the consumption of spectrum resources, visible light communication (VLC) has become the development direction of the next generation communication network with its huge spectrum resources, high security, low cost, and so on [3–5]. The orthogonal frequency division multiplexing (OFDM) technology has the advantages of high spectrum utilization and strong ability of resisting inter-symbol interference (ISI) [6,7]. Hence, the OFDM technology is also an excellent choice for VLC.

Considerable research has applied OFDM technology to VLC. As we all know, the VLC requires non-negative and real OFDM signals, due to intensity modulated direct detection (IM/DD) is widely used in VLC systems [8–10]. In order to meet the requirement, several optical OFDM schemes have been proposed for IM/DD VLC systems. Asymmetrically clipped optical OFDM (ACO-OFDM), where only the odd subcarriers are modulated to transmit the information data, achieves high power efficiency [11]. Pulse amplitude modulated discrete multitone (PAM-DMT) is one of clipping-based schemes, where only the imaginary parts of the subcarriers are used, while the real parts are set to zero [12].

However, due to half of the subcarrier resources not being utilized, the ACO-OFDM and PAM-DMT schemes lead to a significant loss of spectral efficiency [13].

Hence, some advanced schemes superimposing various optical OFDM components have been proposed to improve spectral efficiency, including hybrid asymmetrically clipped optical OFDM (HACO-OFDM) [14] with pulse-amplitude-modulated based hybrid optical OFDM (PHO-OFDM) [15] and adaptively biased optical OFDM (ABO-OFDM) [16]. The ACO-OFDM signals and PAM-DMT signals are transmitted simultaneously in HACO-OFDM scheme, where high spectrum efficiency is achieved compared with the ACO-OFDM and PAM-DMT schemes. However, the interference of the clipping of the bipolar signal falls on the superimposed components. The operation of mitigating the interference at the receiver leads to a significantly high receiver complexity [17]. Similarly, the PAM signals and the QAM signals are transmitted on odd and even subcarriers in the PHO-OFDM scheme, respectively. Unfortunately, the clipping noise of the PAM signals affects the demodulation of the QAM signals that are modulated on the even subcarriers, which significantly increase the complexity of the receiver. Another advanced scheme, known as ABO-OFDM, uses the odd and a part of the even subcarriers to convey the information data, which enhances the spectral efficiency compared to ACO-OFDM scheme. Nevertheless, the reserved subcarriers are not utilized, which incurs a bandwidth penalty.

In this paper, a novel hybrid adaptive bias optical OFDM (HABO-OFDM) scheme is conceived to enhance spectral efficiency with power efficiency, and achieve low-complexity implementation of the receiver. Our main contributions are as follows:

- A novel structure combining different optical OFDM components to transmit the signals simultaneously is proposed for VLC. This structure occupies all subcarriers to convey the signals, thus significantly enhancing the spectral efficiency in comparison with ABO-OFDM.
- The adaptive bias is carefully designed to guarantee the non-negativity of the transmitted signal and improve power efficiency. Furthermore, since the interference caused by the adaptive bias does not disturb the estimation of the superimposed signals at the receiver, a relatively simple receiver can be employed in HABO-OFDM.
- Different performances analysis of our proposed system is presented. We show its performance and perform analysis by comparing the proposed scheme with HACO-OFDM and ABO-OFDM in terms of bit error rate (BER), peak-to-average-power ratio (PAPR), and power efficiency performances. In addition, the BER performance under nonlinear conditions is also demonstrated.

This paper is organized as follows. Section 2 describes the transmitter and receiver in the HABO-OFDM scheme in detail. Additionally, it presents the design of the adaptive bias and the proof that the noise introduced by the adaptive bias does not affect the demodulation of the superimposed signals. Section 3 analyzes the complexity of HABO-OFDM and conventional superimposed schemes, including HACO-OFDM and PHO-OFDM. The results of the different schemes performance are shown in Section 4. We provide the BER performance of these schemes in the additive white Gaussian noise (AWGN) channel. We also provide a comparison of the performances of the PAPR and power efficiency for these schemes. In Section 5, we draw conclusions for the proposed scheme.

2. System Model

In this section, the transmitter and receiver of the proposed HABO-OFDM scheme are investigated concretely. In addition, the adaptive bias is also introduced specifically.

2.1. Transmitter

The block diagram structure of the transmitter of the proposed HABO-OFDM system is presented in Figure 1.

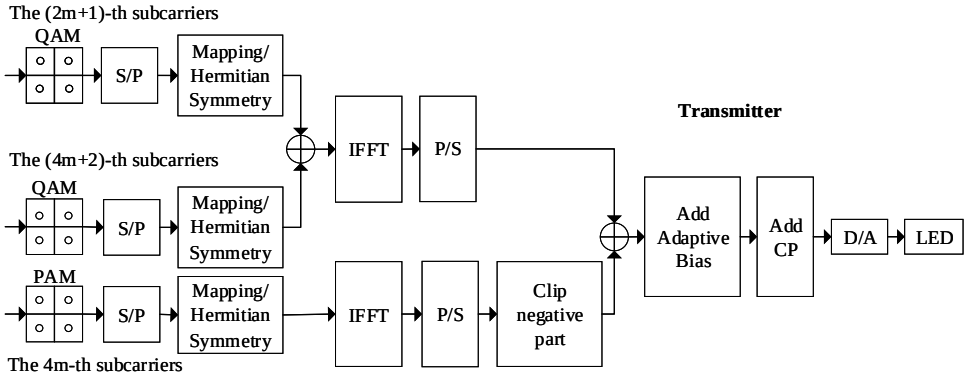

Figure 1. Block diagram structure of the transmitter of the proposed HABO-OFDM system.

In the proposed scheme, for the $(2m + 1)$-th $(m = 0, 1, \cdots, N/8 - 1)$ subcarriers, the transmitted signal is mapped in line with the Hermitian symmetry [11]. Thus, the frequency-domain signal of this component is expressed as

$$\mathbf{X}_1 = [0, Q_1, 0, Q_2, 0, \cdots, Q_{N/4}, 0, Q^*_{N/4}, 0, \cdots, Q^*_2, 0, Q^*_1], \tag{1}$$

where N is the number of subcarriers, and Q_i is the quadrature amplitude modulation (QAM) symbol. For the $(4m + 2)$-th $(m = 0, 1, \cdots, N/8 - 1)$ subcarriers, the modulation of the transmitted signal is QAM. Hence, the frequency-domain signal is given as follows:

$$\mathbf{X}_2 = [0, 0, Q_{N/4+1}, 0, \cdots, Q_{3N/8}, 0, 0, 0, Q^*_{3N/8}, \cdots, 0, Q^*_{N/4+1}, 0], \tag{2}$$

where Q_i denotes the QAM symbol. Furthermore, the modulated transmission signals in $\mathbf{X}_1$ and $\mathbf{X}_2$ are allocated on different subcarriers. Then, the frequency-domain signal of the superimposition of two different component is given by

$$\mathbf{X} = [0, Q_1, Q_{N/4+1}, Q_2, 0, \cdots, Q_{3N/8}, Q_{N/4}, 0, Q^*_{N/4}, Q^*_{3N/8}, \cdots, 0, Q^*_{N/4+1}, 0], \tag{3}$$

where Q_i is the QAM symbol.

The remaining component in HABO-OFDM only modulates the imaginary parts of the $4m$-th $(m = 0, 1, \cdots, N/8 - 1)$ subcarriers, which can be presented as

$$\mathbf{Y} = j[0, 0, 0, 0, P_1, 0, \cdots, P_{N/8-1}, 0, 0, 0, 0, 0, 0, 0, P^*_{N/8-1}, 0, \cdots, 0, P^*_1, 0, 0, 0], \tag{4}$$

where $Y_{4k} = jP_k$ and P_k represents the real PAM symbol, $k = 1, \cdots, N/2 - 1$. Additionally, the time-domain signal y_n holds anti-symmetry and periodic property [18],

$$\begin{cases} y_0 = y_{N/4} = y_{N/2} = y_{3N/4} = 0, \\ y_n = y_{n+N/2} = -y_{N/2-n} = -y_{N-n}, \quad n = 1, 2, \cdots, N/4 - 1 \end{cases}. \tag{5}$$

Therefore, the combined time-domain signal w_n of the proposed scheme, is as follows:

$$w_n = x_n + \lfloor y_n \rfloor, \quad n = 0, 1, \cdots, N - 1, \tag{6}$$

where x_n denotes the time-domain signal of $\mathbf{X}$, and $\lfloor y_n \rfloor_c = \max\{y_n, 0\}$ presents the clipped value of y_n. Thus, x_n does not interfere with the $4m$-th subcarriers of the PAM component due to x_n is unclipped. Moreover, the interference generated by $\lfloor y_n \rfloor$ only falls on the real parts of the $4m$-th subcarriers, which implies that the $(2m + 1)$-th and the $(4m + 2)$-th subcarriers with the imaginary parts of the $4m$-th subcarriers are not interfered with the clipping operation of y_n. The combination of QAM and PAM achieves the advantage of high spectral efficiency. However, the hybrid optical OFDM signal of w_n is a bipolar signal, and it is necessary to ensure the non-negativity of the signal in the optical OFDM

scheme [19]. In order to guarantee the non-negativity of w_n, we design the adaptive bias according to the characteristics of the superimposed signal. Furthermore, the properties which are satisfied with the adaptive bias s_n can be expressed as

$$\begin{aligned} &s_n = s_{n+N/4} = s_{n+N/2} = s_{n+3N/4} = -\min\{w_n, w_{n+N/4}, w_{n+N/2}, w_{n+3N/4}\}, \\ &n = 0, N/8, \end{aligned} \tag{7}$$

$$\begin{aligned} &s_n = s_{N/4-n} = s_{N/4+n} = s_{N/2-n} = s_{N/2+n} = s_{3N/4-n} = s_{3N/4+n} = s_{N-n} \\ &\quad = -\min\{w_n, w_{N/4-n}, w_{N/4+n}, w_{N/2-n}, w_{N/2+n}, w_{3N/4-n}, w_{3N/4+n}, w_{N-n}\}, \\ &n = 1, \cdots, N/8-1 \end{aligned} \tag{8}$$

According to (7), it is obvious that, when at least one of the four signals, w_n, $w_{n+N/4}$, $w_{n+N/2}$, $w_{n+3N/4}$, for $n = 0, N/8$ is negative, the inverse polarity of the minimum of $\{w_n, w_{n+N/4}, w_{n+N/2}, w_{n+3N/4}\}$ can be selected to produce the adaptive bias. Additionally, if the four signals are all non-negative, no bias is required to ensure the non-negativity of the four signals.

From (8), if at least one signal in $\{w_n, w_{N/4-n}, w_{N/4+n}, w_{N/2-n}, w_{N/2+n}, w_{3N/4-n}, w_{3N/4+n}, w_{N-n}\}$ for $n = 1, \cdots, N/8-1$ is negative, the adaptive bias can be generated with the inverse polarity of the minimum of $\{w_n, w_{N/4-n}, w_{N/4+n}, w_{N/2-n}, w_{N/2+n}, w_{3N/4-n}, w_{3N/4+n}, w_{N-n}\}$. In addition, if the eight signals are all non-negative, there is no need to produce the adaptive bias. Furthermore, it can also be observed that adaptive bias is selected according to the different amplitude of the signal, which can decrease the power consumption, and still ensure the non-negativity of the signal.

As a result, the superimposed time-domain signal of the proposed scheme is given by

$$z_n = w_n + s_n, \quad n = 0, 1, \cdots, N-1. \tag{9}$$

Through the introduction of the adaptive bias, the non-negativity of the transmission signal is dynamically adjusted to realize the simultaneous transmission of different optical OFDM signals, while maintaining high spectrum utilization.

2.2. Receiver

Now, we discuss the demodulation process of the proposed HABO-OFDM scheme. The block diagram structure of the receiver of the proposed HABO-OFDM system is shown in Figure 2.

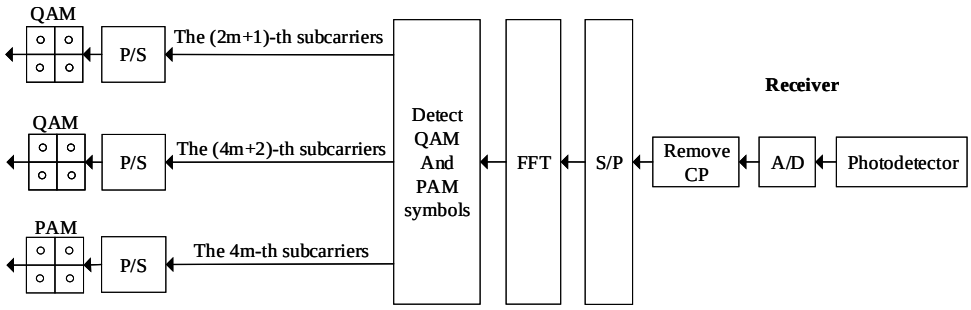

Figure 2. Block diagram structure of the receiver of the proposed HABO-OFDM system.

It can be obtained that x_n occupies the $(2m + 1)$-th and $(4m + 2)$-th subcarriers, and $\lfloor y_n \rfloor_c$ occupies the imaginary parts of the $4m$ subcarriers in HABO-OFDM scheme. The clipping noise of y_n only falls on the real parts of the $4m$ subcarriers, and there is no interference to x_n. Meanwhile, no clipping noise generated by x_n is superimposed on the imaginary parts of the $4m$ subcarrier of $\lfloor y_n \rfloor_c$ owing to no clipping operation for x_n. Therefore, the two sets of signals have no influence on each other during demodulation. Furthermore, the following will prove that the adaptive bias will not cause interference to the transmission signals x_n and $\lfloor y_n \rfloor_c$.

Specifically, the equation obtained by expanding the Fast Fourier transform (FFT) of s_n can be expressed as

$$\begin{aligned} S_k = \frac{1}{\sqrt{N}} \sum_{n=0}^{N-1} s_n e^{-j\frac{2\pi nk}{N}} &= s_0(1 + e^{-j\frac{\pi k}{2}} + e^{-j\pi k} + e^{-j\frac{3\pi k}{2}}) \\ &+ s_{\frac{N}{8}} e^{-j\frac{\pi k}{4}}(1 + e^{-j\frac{\pi k}{2}} + e^{-j\pi k} + e^{-j\frac{3\pi k}{2}}) \\ &+ \frac{1}{\sqrt{N}} \sum_{n=0}^{\frac{N}{8}-1} s_n[(1 + e^{-j\frac{\pi k}{2}} + e^{-j\pi k} + e^{-j\frac{3\pi k}{2}})e^{-j\frac{2\pi nk}{N}} \\ &+ (1 + e^{-j\frac{\pi k}{2}} + e^{-j\pi k} + e^{-j\frac{3\pi k}{2}})e^{j\frac{2\pi nk}{N}}] \\ k = 0, 1, \cdots, N-1 & \end{aligned} \quad . \tag{10}$$

When k is odd, that is, when $k = 2m + 1$, we can obtain $e^{-j\pi k} = -1$. Then, S_k can be given by

$$\begin{aligned} S_k &= s_0 e^{-j\frac{\pi k}{2}}(1 + e^{-j\pi k}) + s_{\frac{N}{8}} e^{-j\frac{\pi k}{4}} e^{-j\frac{\pi k}{2}}(1 + e^{-j\pi k}) \\ &+ \frac{1}{\sqrt{N}} \sum_{n=1}^{\frac{N}{8}-1} s_n[(1 + e^{-j\pi k})e^{-j\frac{2\pi nk}{N}} e^{-j\frac{\pi k}{2}} + (1 + e^{-j\pi k})e^{j\frac{2\pi nk}{N}} e^{-j\frac{\pi k}{2}}]. \\ &= 0 \end{aligned} \tag{11}$$

When k is even, we can obtain $e^{-j\pi k} = 1$. Thus, S_k can be expressed as the following two cases.

case 1 when $k = 4m + 2$,

$$\begin{aligned} S_k &= s_0(1 + e^{-j(2m+1)\pi} + 1 + e^{-j3(2m+1)\pi}) \\ &+ s_{\frac{N}{8}} e^{-j\frac{\pi}{2}(2m+1)}(1 + e^{-j(2m+1)\pi} + 1 + e^{-j3(2m+1)\pi}) \\ &+ \frac{1}{\sqrt{N}} \sum_{n=1}^{\frac{N}{8}-1} s_n[(1 + e^{-j(2m+1)\pi} + 1 + e^{-j3(2m+1)\pi})e^{-j\frac{4(2m+1)n\pi}{N}} \\ &+ (1 + e^{-j(2m+1)\pi} + 1 + e^{-j3(2m+1)\pi})e^{j\frac{4(2m+1)n\pi}{N}}] \\ &= 0, \end{aligned} \tag{12}$$

case 2 when $k = 4m$,

$$\begin{aligned} S_k &= s_0(1 + e^{-j2m\pi} + e^{-j4m\pi} + e^{-j6m\pi}) \\ &+ s_{\frac{N}{8}} e^{-jm\pi}(1 + e^{-j2m\pi} + e^{-j4m\pi} + e^{-j6m\pi}) \\ &+ \frac{1}{\sqrt{N}} \sum_{n=1}^{\frac{N}{8}-1} s_n(1 + e^{-j2m\pi} + e^{-j4m\pi} + e^{-j6m\pi})e^{-j\frac{8mn\pi}{N}} \\ &+ \frac{1}{\sqrt{N}} \sum_{n=1}^{\frac{N}{8}-1} s_n(1 + e^{-j2m\pi} + e^{-j4m\pi} + e^{-j6m\pi})e^{j\frac{8mn\pi}{N}} \\ &= 4s_0 + 4s_{\frac{N}{8}} e^{-jm\pi} + \frac{4}{\sqrt{N}} \sum_{n=1}^{\frac{N}{8}-1} s_n(e^{-j\frac{8mn\pi}{N}} + e^{j\frac{8mn\pi}{N}}) \\ &= 4s_0 + 4s_{\frac{N}{8}} \cos(m\pi) + \frac{8}{\sqrt{N}} \sum_{n=1}^{\frac{N}{8}-1} s_n \cos(\frac{8mn\pi}{N}) \end{aligned} \quad . \tag{13}$$

Consequently, S_k can be given by

$$S_k = \begin{cases} 0, & k = 2m+1, \\ 0, & k = 4m+2, \\ 4s_0 + 4s_{\frac{N}{8}} \cos(m\pi) + \frac{8}{\sqrt{N}} \sum_{n=1}^{\frac{N}{8}-1} s_n \cos(\frac{8mn\pi}{N}), & k = 4m \end{cases} \quad (14)$$

where $m = 0, 1, \cdots, N/8 - 1$. It can be easily observed that S_k only falls on the real parts of the $4m$-th subcarriers, which explains that the adaptive bias s_n does not disturb x_n and $\lfloor y_n \rfloor_c$. Therefore, a relatively simple OFDM receiver structure can be applied to HABO-OFDM scheme.

3. Complexity Analysis

We will compare the complexity of HABO-OFDM with HACO-OFDM and PHO-OFDM in this section. It is known that the complexity of the transmitter in the conventional optical OFDM scheme is determined by the number of Inverse Fast Fourier Transform (IFFT) operations [20]. In this way, we can evaluate the system complexity by using the number of the real multiplication operation in IFFT [21]. As for HABO-OFDM, the transmitter of it requires an N-point IFFT and another N-point IFFT used on the imaginary value, which yields $3N \log_2 N - 3N + 4$ times of the real multiplication operation. Similarly, $3N \log_2 N - 3N + 4$ times of the real multiplication operation are required for the HACO-OFDM transmitter, which is the same as PHO-OFDM.

As far as the complexity of the receiver, only one N-point FFT and one N-point real-valued FFT are included in HABO-OFDM. Thus, it results in $3N \log_2 N - 3N + 4$ times of the real multiplication operation for the HABO-OFDM receiver. By contrast, the HACO-OFDM receiver needs an N-point FFT and two N-point real-valued FFT, which causes $4N \log_2 N - 6N + 8$ times of the real multiplication operation. In addition, two N-point FFT and one N-point real-valued FFT are needed for the receiver of PHO-OFDM, which leads to $5N \log_2 N - 3N + 4$ times of the real multiplication operation. The comparison of the complexity of the superimposed optical OFDM schemes is shown in Table 1. It can be clearly observed that the complexity of the receiver of the proposed HABO-OFDM scheme is relatively reduced compared with the other two superimposed schemes. Compared with HACO-OFDM and PHO-OFDM, the complexity of the receiver of the proposed scheme is reduced by $N \log_2 N - 3N + 4$ and $2N \log_2 N$, respectively.

Table 1. Comparison of the complexity of the transmitter and receiver of different optical OFDM schemes.

Modulation	Transmitter	Receiver
HABO-OFDM	$3N \log_2 N - 3N + 4$	$3N \log_2 N - 3N + 4$
HACO-OFDM	$3N \log_2 N - 3N + 4$	$4N \log_2 N - 6N + 8$
PHO-OFDM	$3N \log_2 N - 3N + 4$	$5N \log_2 N - 3N + 4$

4. Simulation Results

In this section, we evaluate the performance of the proposed HABO-OFDM scheme through simulation results, and compare it with HACO-OFDM and ABO-OFDM. In the simulation, the number of subcarriers is 512 for these schemes, while the constellation sizes of QAM and PAM symbols are set to M and $\sqrt{M}$, respectively. For HACO-OFDM, we choose 16QAM-4PAM, 64QAM-8PAM, 256QM-16QAM, 1024QAM-32PAM, and 4096QAM-64PAM as simulation conditions. In ABO-OFDM, 16QAM, 64QAM, 256QM, 1024QAM, and 4096QAM are selected as simulation conditions. For HABO-OFDM, we generate signals from M-QAM and $\sqrt{M}$-PAM constellations, such as 16QAM-4PAM, 64QAM-8PAM, 256QM-16PAM, and 1024QAM-32PAM. Additionally, the total average electric power is normalized in different schemes. The system specifications is shown in Table 2. The bit error rate (BER) and peak-to-average-power ratio (PAPR) of the proposed HABO-OFDM

scheme are calculated and compared with HACO-OFDM and ABO-OFDM. We also present the BER performance of the three schemes in the nonlinearity limit. Moreover, calculation results in the electric power efficiency of the proposed HABO-OFDM scheme with HACO-OFDM and ABO-OFDM are also shown.

Table 2. System specifications.

Name of Parameters	Values
The number of subcarriers	512
The constellation sizes of QAM	16, 64, 256, 1024, 4096
The constellation sizes of PAM	4, 8, 16, 32, 64
The clipping ratio τ	9 dB
The BER target	10^{-3}

Figure 3 shows the BER curves of QAM and PAM with different constellation sizes in HACO-OFDM, ABO-OFDM and the proposed HACO-OFDM scheme. It can be observed that HACO-OFDM and ABO-OFDM nearly present the same BER performance. Simultaneously, we also see that the BER performance of the proposed HABO-OFDM scheme is slightly degraded compared with the other two schemes. This is on account of the proposed HABO-OFDM scheme, where part of the power is allocated to the reserved subcarriers that are modulated at the same time, which in the ABO-OFDM scheme are not utilized. In addition, the proposed HABO-OFDM scheme can transmit more information data than HACO-OFDM under the same simulation conditions, which explains that the BER performance of HABO-OFDM is slightly worse than that of HACO-OFDM. In fact, for 256QAM-16PAM, the spectral efficiency of HABO-OFDM is improved to 7 bit/s/Hz, while the other two schemes are 6 bit/s/Hz. Specifically, this is about a 16.6% enhancement. Therefore, the spectral efficiency of the proposed HABO-OFDM scheme has been relatively improved compared with the other two systems.

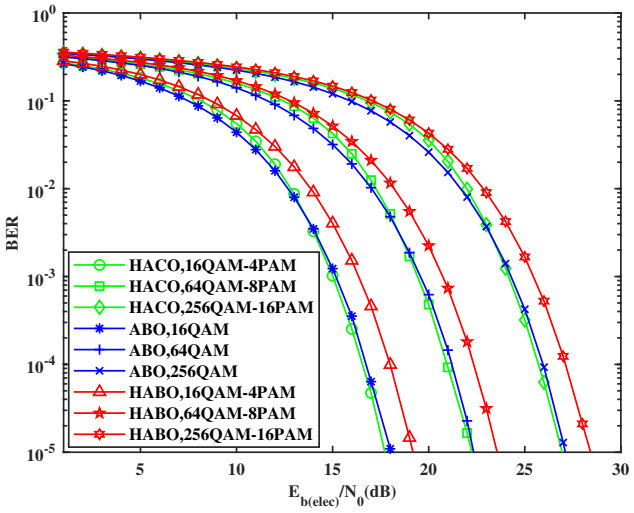

Figure 3. Comparison of the BER performance for HACO-OFDM, ABO-OFDM, and HABO-OFDM.

The complementary cumulative distribution function (CCDF) curves of the PAPR for different schemes are shown in Figure 4. We can clearly observe that the PAPR of HABO-OFDM has a significant reduction compared with HACO-OFDM and ABO-OFDM, which means that the influence of nonlinear distortion is greatly alleviated [22]. Specifically, there is about a 3.2 dB reduction in the PAPR compared to HACO-OFDM, and it is reduced by about 1.7 dB in comparison to ABO-OFDM.

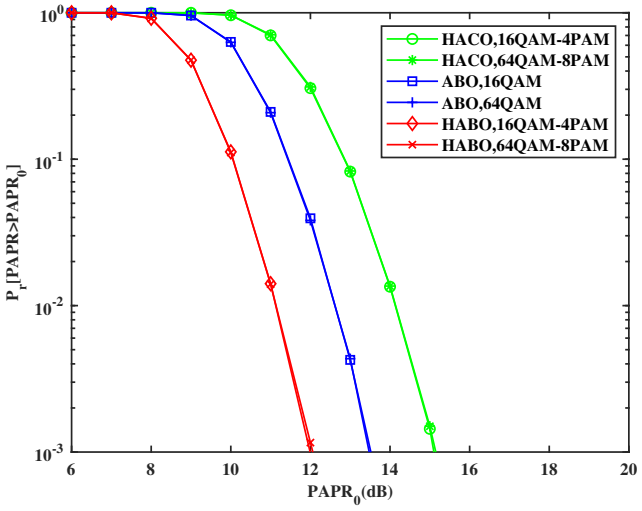

Figure 4. CCDF curves of the PAPR for HACO-OFDM, ABO-OFDM, and HABO-OFDM.

Figure 5 presents the BER performance of HACO-OFDM, ABO-OFDM, and HABO-OFDM under the nonlinear constraints, where the clipping ratio τ is set to 9 dB [23]. It is clear that the anti-nonlinearity ability of HABO-OFDM is noticeably improved compared with HACO-OFDM and ABO-OFDM. Thanks to the fact that PAPR of HABO-OFDM is superior to HACO-OFDM and ABO-OFDM, HABO-OFDM obtains significantly better BER performance.

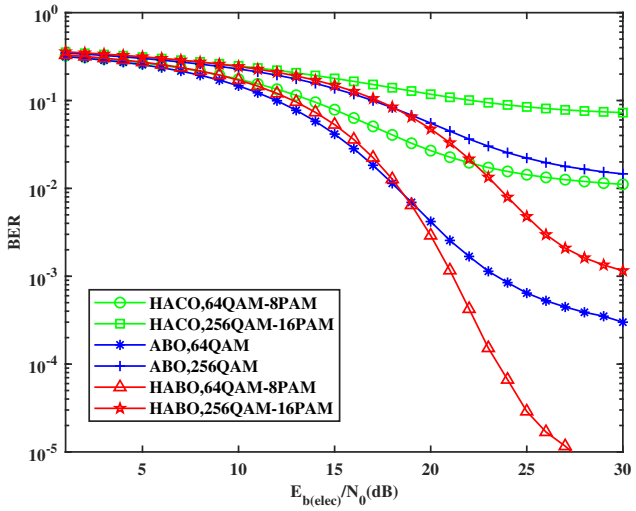

Figure 5. BER of HACO-OFDM, ABO-OFDM, and HABO-OFDM versus $E_{b(elec)}/N_0$ when the clipping ratio is set to 9 dB.

The variation of $\langle E_{b(elec)}/N_0\rangle_{BER}$ when the proportion of electric energy allocated to subcarriers using QAM ranges from 0.1 to 0.9 is shown in Figure 6. We choose the size of QAM constellation and PAM constellation to be M and $\sqrt{M}$. In this way, it is shown that the minimum $\langle E_{b(elec)}/N_0\rangle_{BER}$ is obtained when the proportion of electric power allocated to subcarriers using QAM is 0.6 for all cases.

In Figure 7, the $\langle E_{b(elec)}/N_0\rangle_{BER}$ versus the proportion of electric power allocated to subcarriers using QAM is presented. The size of QAM constellation and PAM constellation is defined as M and $\sqrt{M}$. The minimum $\langle E_{b(elec)}/N_0\rangle_{BER}$ is achieved when the proportion of electric power on subcarriers using QAM is 0.7 in all cases. This is because, in

HABO-OFDM, the subcarriers that use QAM to modulate the transmitted signal occupy the majority.

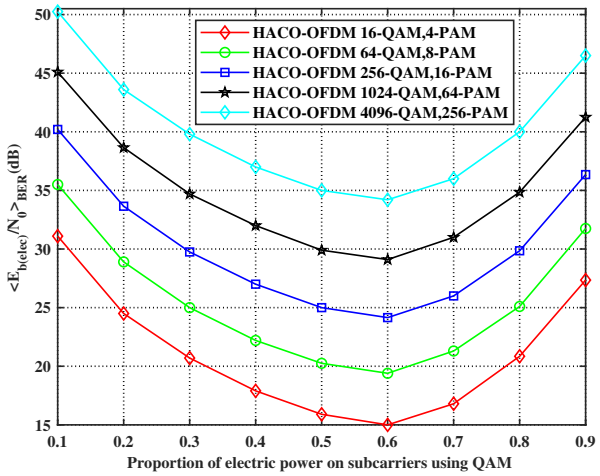

Figure 6. Comparison of $\langle E_{b(elec)}/N_0\rangle_{BER}$ for HACO-OFDM for different proportions of electric power.

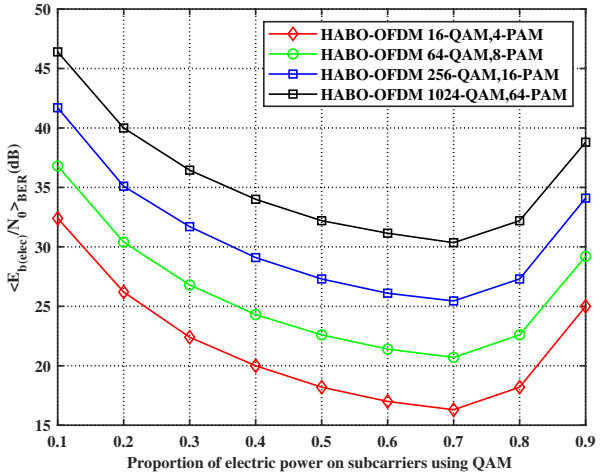

Figure 7. Comparison of $\langle E_{b(elec)}/N_0\rangle_{BER}$ for HABO-OFDM for different proportions of electric power.

In Figure 8, the required $E_{b(elec)}/N_0$ for the BER target of 10^{-3} versus Bit rate/Normalized bandwidth [24] is presented. In order to make a fair comparison, the average electric power of each of the three schemes is set to be uniform. Since HACO-OFDM and HABO-OFDM are combined modulations of QAM and PAM, the distribution of electric power needs to be considered. The $\langle E_{b(elec)}/N_0\rangle_{BER}$ versus the proportion of electric power allocated to subcarriers using QAM for HACO-OFDM and HABO-OFDM is shown in Figures 6 and 7, respectively. Therefore, the lowest values of $\langle E_{b(elec)}/N_0\rangle_{BER}$ for HACO-OFDM and HABO-OFDM can be selected.

From Figure 8, we see that the Bit rate/Normalized bandwidth of 3, 4.5, 6, 7.5, 9 for HACO-OFDM and ABO-OFDM and the Bit rate/Normalized bandwidth of 3.5, 5.25, 7, 8.75 for HABO-OFDM are shown. We can clearly obtain that when the Bit rate/Normalized bandwidth is in the range of 3 to 9, the $E_{b(elec)}/N_0$ required for HACO-OFDM and ABO-OFDM to achieve the BER target of 10^{-3} is almost the same, which means that their power efficiency is similar. Moreover, it is obvious that as the Bit rate/Normalized bandwidth increases, the $E_{b(elec)}/N_0$ required for HABO-OFDM to achieve the BER target of 10^{-3} will

be significantly lower than the other two schemes, which shows that in a wide range of the Bit rate/Normalized bandwidth, HABO-OFDM exhibits higher power efficiency in comparison with HACO-OFDM and ABO-OFDM.

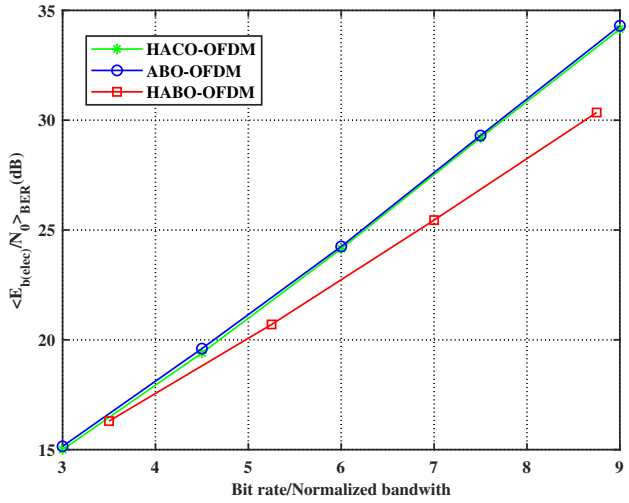

Figure 8. $\langle E_{b(elec)}/N_0\rangle_{BER}$ required for the BER target of 10^{-3} versus Bit rate/Normalized bandwidth.

5. Conclusions

In this paper, a novel HABO-OFDM scheme was proposed for VLC to achieve the high spectrum efficiency and power efficiency. In terms of 256QAM-16PAM, we saw about a 16.6% enhancement in spectrum efficiency compared with the other two schemes. Compared with the conventional superimposed systems, the complexity of the HABO-OFDM receiver was significantly reduced due to the introduction of adaptive bias, which not only had no interference to the transmitted signal but also guaranteed the non-negativity of the signal. Specifically, the complexity of the HABO-OFDM receiver was reduced by $N\log_2 N - 3N + 4$ and $2N\log_2 N$ compared to HACO-OFDM and PHO-OFDM. Meanwhile, HABO-OFDM had a superior PAPR performance in comparison with HACO-OFDM and ABO-OFDM. There was about a 3.2 dB reduction and 1.7 dB reduction in PAPR compared with HACO-OFDM and ABO-OFDM. Additionally, HABO-OFDM also maintained a better power efficiency performance than HACO-OFDM and ABO-OFDM in a wide range of the Bit rate/Normalized bandwidth. However, in the proposed scheme, the real parts of some subcarriers were still not used. We will continue to exploit the reserved parts in future researches. Furthermore, the proposed HABO-OFDM scheme can be applied in high-speed VLC in future due to its high spectral efficiency, low receiver complexity, low PAPR, and high power efficiency.

Author Contributions: Conceptualization, H.H.; methodology, H.H.; software, H.H.; validation, H.H., Z.L.; formal analysis, H.H.; investigation, H.H.; resources, H.H.; data curation, H.H.; writing—original draft preparation, H.H.; writing—review and editing, Z.L.; visualization, H.H.; supervision, Z.L.; project administration, Z.L.; funding acquisition, Z.L. All authors have read and agreed to the published version of the manuscript.

Funding: This research was funded by the National Natural Science Foundation of China under Grant 61571108; in part by the Wuxi Science and Technology Development Fund(No.H20191001, No.G20192010); in part by the Natural Science Foundation of Jiangsu Province under Grants BK20190582.

Institutional Review Board Statement: Not applicable.

Informed Consent Statement: Not applicable.

Data Availability Statement: Not applicable.

Conflicts of Interest: The authors declare no conflict of interest.

References

1. Zafar, F.; Karunatilaka, D.; Parthiban, R. Dimming Schemes for Visible Light Communication: The State of Research. *IEEE Wireless Commun.* **2015**, *22*, 29–35. [CrossRef]
2. Khan, L.U. Visible Light Communication: Applications, Architecture, Standardization and Research Challenges. *Digit. Commun. Netw.* **2017**, *3*, 78–88. [CrossRef]
3. Wu, S.; Wang, H.; Youn, C. Visible Light Communications for 5G Wireless Networking Systems: From Fixed to Mobile Communications. *IEEE Netw.* **2014**, *28*, 41–45. [CrossRef]
4. Khalid, A.; Asif, H.M.; Kostromitin, K.I.; Al-Otaibi, S.; Huq, K.M.S.; Rodriguez, J. Doubly Orthogonal Wavelet Packets for Multi-Users Indoor Visible Light Communication Systems. *Photonics* **2019**, *6*, 85. [CrossRef]
5. Haas, H.; Yin, L. Physical-Layer Security in Multiuser Visible Light Communication Networks. *IEEE J. Sel. Areas Commun.* **2018**, *36*, 162–174.
6. Islim, M.S.; Ferreira, R.X.; He, X.Y.; Xie, E.Y.; Videv, S.; Viola, S.; Watson, S.; Bamiedakis, N.; Penty, R.V.; White, I.H.; et al. Towards 10Gb/s Orthogonal Frequency Division Multiplexing-Based Visible Light Communication Using A GaN Violet Micro-LED. *Photon. Res.* **2017**, *5*, A35–A43. [CrossRef]
7. Başar, E.; Aygölü, Ü.; Panayırcı, E.; Poor, H.V. Orthogonal Frequency Division Multiplexing with Index Modulation. *IEEE Trans. Signal Process.* **2013**, *61*, 5536–5549. [CrossRef]
8. Armstrong, J.; Schmidt, B.J.C. Comparison of Asymmetrically Clipped Optical OFDM and DC-Biased Optical OFDM in AWGN. *IEEE Commun. Lett.* **2008**, *12*, 343–345. [CrossRef]
9. Armstrong, J.; Lowery, A.J. Power Efficient Optical OFDM. *Electron. Lett.* **2006**, *42*, 370–372. [CrossRef]
10. Le-Tran, M.; Kim, S. Deep Learning-Assisted Index Estimator for Generalized LED Index Modulation OFDM in Visible Light Communication. *Photonics* **2021**, *8*, 168. [CrossRef]
11. Xu, W.; Wu, M.; Zhang, H.; You, X.; Zhao, C. ACO-OFDM-Specified Recoverable Upper Clipping with Efficient Detection for Optical Wireless Communications. *IEEE Photon. J.* **2014**, *6*, 1–17.
12. Lee, S.C.J.; Randel, S.; Breyer, F.; Koonen, A.M.J. PAM-DMT for Intensity-Modulated and Direct-Detection Optical Communication Systems. *IEEE Photon. Technol. Lett.* **2009**, *21*, 1745–1749. [CrossRef]
13. Li, B.L.; Feng, S.; Xu, W. Spectrum-Efficient Hybrid PAM-DMT for Intensity-Modulated Optical Wireless Communication. *Opt. Exp.* **2020**, *28*, 12621–12637. [CrossRef]
14. Ranjha, B.; Kavehrad, M. Hybrid Asymmetrically Clipped OFDM-Based IM/DD Optical Wireless System. *IEEE/OSA J. Opt. Commun. Netw.* **2014**, *6*, 387–396. [CrossRef]
15. Zhang, T.; Zou, Y.; Sun, J.; Qiao, S. Design of PAM-DMT-Based Hybrid Optical OFDM for Visible Light Communications. *IEEE Wirel. Commun. Lett.* **2019**, *8*, 265–268. [CrossRef]
16. Li, B.L.; Xu, W.; Li Z.; Zhou Y. Adaptively Biased OFDM for IM/DD-Aided Optical Wireless Communication Systems. *IEEE Wireless Commun. Lett.* **2020**, *9*, 698–701. [CrossRef]
17. Li, B.L.; Xue, X.; Feng, S.; Xu, W. Layered Optical OFDM with Adaptive Bias for Dimming Compatible Visible Light Communications. *J. Lightw. Technol.* **2021**, *39*, 3434–3444. [CrossRef]
18. Wang, T.; Hou, Y.; Ma, M. A Novel Receiver Design for HACO-OFDM by Time-Domain Clipping Noise Elimination. *IEEE Commun. Lett.* **2018**, *22*, 1862–1865. [CrossRef]
19. Yesilkaya, A.; Bian, R.; Tavakkolnia, I.; Haas, H. OFDM-Based Optical Spatial Modulation. *IEEE J. Sel. Top. Signal Process.* **2019**, *13*, 1433–1444. [CrossRef]
20. Wang, Q.; Qian, C.; Guo, X.; Wang, Z.; Cunningham, D.G.; White, I.H. Layered ACO-OFDM for Intensity-Modulated Direct-Detection Optical Wireless Transmission. *Opt. Exp.* **2015**, *23*, 12382–12393. [CrossRef]
21. Liu, C.; Chan, C.; Cheng, P.; Lin, H. FFT-Based Multi-Rate Signal Processing for 18-Band Quasi-ANSI S1.11 1/3-Octave Filter Bank. *IEEE Trans. Circuits Syst. II Exp. Briefs* **2019**, *66*, 878–882. [CrossRef]
22. Mestdagh, D.J.G.; Monsalve, J.L.; Brossier, J.M. GreenOFDM: A New Selected Mapping Method for OFDM PAPR Reduction. *Electron. Lett.* **2018**, *54*, 449–450. [CrossRef]
23. Li, B.; Xu, W.; Zhang, H.; Zhao, C.; Hanzo, L. PAPR Reduction for Hybrid ACO-OFDM Aided IM/DD Optical Wireless Vehicular Communications. *IEEE Trans. Veh. Technol.* **2017**, *66*, 9561–9566. [CrossRef]
24. Armstrong, J.; Dissanayake, S.D. Comparison of ACO-OFDM, DCO-OFDM and ADO-OFDM in IM/DD Systems. *J. Lightw. Technol.* **2013**, *31*, 1063–1072.